Dyes and Pigments 150 (2018) 121–129

Contents lists available at ScienceDirect

Dyes and Pigments

journal homepage: www.elsevier.com/locate/dyepig

Synthesis, luminescent properties and theoretical calculations of novel orange-red-emitting $Ca_2Y_8(SiO_4)_6O_2:Sm^{3+}$ phosphors for white light-emitting diodes

Chun-Ting Chen[a,b], Tzu-Jen Lin[a], Maxim S. Molokeev[c,d,e], Wei-Ren Liu[a,*]

[a] Department of Chemical Engineering, Chung Yuan Christian University, Chung Li, Taiwan
[b] National Chung Shan Institute of Science & Technology, Taoyuan, Taiwan
[c] Laboratory of Crystal Physics, Kirensky Institute of Physics, Federal Research Center KSC SB RAS, Krasnoyarsk 660036, Russia
[d] Department of Physics, Far Eastern State Transport University, Khabarovsk 680021, Russia
[e] Siberian Federal University, Krasnoyarsk 660079, Russia

ARTICLE INFO

Keywords:
$Ca_2Y_8(SiO_4)_6O_2$
Photoluminescence
Phosphor
Solid state reaction

ABSTRACT

The novel orange-red-emitting $Ca_2Y_8(SiO_4)_6O_2:Sm^{3+}$ phosphors (CYSO:Sm^{3+}) were synthesized via conventional a solid state reaction. The crystal structure and atomic coordinates of CYSO:Sm^{3+} was characterized by Rietveld refinement. Luminesce properties of as-synthesized CYSO:Sm^{3+} phosphors are carried out by PL/PLE, decay life time, thermal quenching as well as reflectance spectrometer and LED fabrications. The results indicates that composition-optimized CYSO:1%Sm^{3+} exhibits orange-red emission peaks located on 564, 601, 608 and 648 nm attributed to the transitions of $^4G_{5/2} \rightarrow {}^6H_{5/2}$, $^4G_{5/2} \rightarrow {}^6H_{7/2}$, $^4G_{5/2} \rightarrow {}^6H_{7/2}$ and $^4G^{5/2} \rightarrow {}^6H_{9/2}$, respectively. The decay lifetime of CYSO:Sm^{3+} phosphors was in the range of 0.37–1.10 ms. The temperature-dependent photoluminescence is decreased to 80% from room temperature to 150 °C, which is superior to that of commercial red phsophpr-$Y_2O_3:Eu^{3+}$. The results of LED fabrication by combing 405 chips and blue/green phosphors are demonstrated in this study. Finally, from viewpoint of theoretical calculations, band structure and density of state for CYSO and CYSO:Sm^{3+} are studied by first principles calculations. All the results indicate that CYSO:Sm^{3+} phosphors could be a potential material for white light-emitting diodes.

1. Introduction

In recent years, white light-emitting diodes (W-LEDs) have drawn much attractions due to their merits of high brightness, environmentally friendly, long lifetime, well energy efficiency and less power consumption [1–4]. Thus, it is considered to be the next generation light source. The traditional W-LEDs are mainly manufactured by combing the blue-emitting InGaN chips with a yellow-emitting phosphor, Ce^{3+}-doped yttrium aluminum garnet (YAG:Ce^{3+}) [5–7]. This approach, however, leads to thermal quenching and fails to achieve higher color rendering index (CRI) because of the lack of red component in blending of different color phosphors [8]. In order to overcome these disadvantages, some approaches could be used, such as adding red-emitting nitride-based phosphors ($Sr_2Si_5N_8:Eu^{2+}$ or $CaAlSiN_3:Eu^{2+}$), oxides [60] or carbon quantum dots [61]. Even though these nitride phosphors have excellent thermal stability. Nevertheless, they have relatively high producing expense because of the patent licensing costs and processes of synthesis which require higher sintering temperature and high pressure [9]. Hence, for above reasons, it is much necessary to develop new red-emitting phosphors which are suitable for n-UV (370–410 nm) or blue chip (~460 nm) to exhibit good thermal stability and lower manufacturing costs for warm light W-LEDs.

Rare earth ions-doped phosphors are considered as the potential photoluminescence materials. Among these rare earth ions, Samarium ions (Sm^{3+}) are demonstrated reddish-orange emission nature under excitation because of the transition of $^4G_{5/2} - {}^6H_J$ (J = 5/2, 7/2, 9/2 and 11/2) [10–12]. Recently, a series of Sm^{3+}-doped phosphors have been reported, such as $BaMoO_4:Sm^{3+}$ [13], $Sr_2ZnSi_2O_7:Sm^{3+}$ [14], $NaCaBO_3:Sm^{3+}$ [15], $KLaSr_3(PO_4)F:Sm^{3+}$ [16], $Na_2CaSn_2Ge_3O_{12}:Sm^{3+}$ [17], $Ca_3Bi(PO_4)_3:Sm^{3+}$ [18] and $Ba_2Ca(BO_3)_2:Sm^{3+}$ [19]. In addition, some literature focusses on Sm^{3+} and Eu^{3+} co-doped to enhance luminesce intensity via energy transfer from Sm^{3+} to Eu^{3+} and to extend both the excitation and emission spectra. For example, $SrBi_2Si_2O_7:Sm^{3+}$, Eu^{3+} [19], $CaGd_2(WO_4)_4:Eu^{3+}$, Sm^{3+} [20], $LaMgAl_{11}O_{19}:Sm^{3+}$, Eu^{3+} [21] and $Na_3YSi_2O_7:Sm^{3+}$, Eu^{3+} [22] have been reported. Lu et al. report $Bi_4Si_3O_{12}:Sm^{3+}$, which were prepared via sol-gel method. It revealed

* Corresponding author.
E-mail address: WRLiu1203@gmail.com (W.-R. Liu).

https://doi.org/10.1016/j.dyepig.2017.10.047
Received 15 September 2017; Received in revised form 16 October 2017; Accepted 31 October 2017
Available online 17 November 2017
0143-7208/

strongest emission peak located at 608 nm due to the transition of $^4G_{5/2}$ – $^6H_{7/2}$ [23]. The optimum doping concentration was 4 mol.% and the diameters of particles reached 2 to 4 μm. Gokhe et al. displayed Sm^{3+}-doped $LiAlSiO_4$ phosphors by a solid state reaction [8]. The particle size and morphology were determined through SEM and the average size was in the range of 2–10 μm. The XDAX were used to realize the presence of element content for as-prepared samples. The CIE coordinate (x = 0.595, y = 0.387) indicated that the phosphors could be a potential candidate for pc-LEDs. Nair et al. discussed the $Ca_3Mg_3(PO_4)_4$:Sm^{3+} phosphors, which were investigated that they emitted orange emission as excited by n-UV and blue light. They found the energy transfer mechanism of that was dipole-dipole interaction [24] and showed three emission peaks attributed to transition of $^4G_{5/2}$ – $^6H_{5/2}$ $^4G_{5/2}$ – $^6H_{7/2}$ and $^4G_{5/2}$ – $^6H_{9/2}$. Besides, Kang et al. reported $Na_2Y_2Ti_3O_{10}$:Eu^{3+}, Sm^{3+} phosphors, which showed a 3-fold higher PL intensity than that of commercial red-emitting Y_2O_2S:Eu^{3+} phosphors upon 396 nm. The Sm^{3+} ions acted as a sensitizer, which increased the PL intensity up to 35% as excited under 410 nm. The fabrication of LEDs were combined with 400 nm chips, which showed the Ra and CCT were 83 and 5556 K, respectively [25].

Phosphors structure with the formula $A_2RE_8(SiO_4)_6O_2$ (A = divalent alkaline-earth metal cation, RE = trivalent rare earth ion) are stable and rigid materials various compositional substitutions of rare earth activators [26–33]. Therefore, we chose this structure to carry out more study.

To the best of our knowledge, Sm^{3+}-doped $Ca_2Y_8(SiO_4)_6O_2$ phosphors have not been reported in the literature. As a result, it is a potential material to be developed in LEDs applications. In this paper, we firstly report the characterization of un-doped and Sm^{3+}-doped $Ca_2Y_8(SiO_4)_6O_2$ phosphors, synthesized via a solid state reaction. To further investigation, the crystal structure was observed by both powder X-ray diffraction and Rietveld refinement. The local crystal structure and bonding of dopant cations would affect the optical properties, which could be obtained through photoluminescence spectra. The theoretical calculation was first studied for $Ca_2Y_8(SiO_4)_6O_2$ phosphors. We also attempted to acquire the properties of color quality of as-prepared phosphors such as CCT, CIE and CRI which are the fundamental to design the luminescent materials. All the results were carefully investigated in detail in this paper.

2. Experimental

2.1. Sample preparation

The $Ca_2Y_8(SiO_4)_6O_2$:Sm^{3+} phosphors were prepared by a conventional solid state reaction. $CaCO_3$ (A.R. 99.99%), Y_2O_3 (A.R. 99.99%), SiO_2 (A.R. 99.99%), Sm_2O_3 (A.A. 99.9%) were used as raw materials to synthesize phosphors. After all the raw materials were ground thoroughly in an agate mortar, the mixtures were placed into alumina crucible, which was heated at 1450 °C for 8 h in air and then cooled down to room temperature naturally.

2.2. Sample characterization

The powder diffraction data of $Ca_2Y_8(SiO_4)_6O_2$:$0.01Sm^{3+}$ for Rietveld analysis was collected at room temperature with a Bruker D8 ADVANCE powder diffractometer (Cu-Kα radiation) and linear VANTEC detector. The step size of 2θ was 0.016°, and the counting time was 2 s per step. The 2θ range of 9-70° was measured with 0.6 mm divergence slit, but 2θ range of 70-140° was measured with 2 mm divergence slit. Larger slits allow noticeably increase intensity of high-angle peaks without loss of resolution because the high-angle peaks are broad enough to be not affected by bigger divergence beam. The esd's $\sigma(I_i)$ of all points on patterns were calculated using intensities I_i: $\sigma(I_i) = I_i^{1/2}$. The intensities and obtained esd's were further normalized: $I_{i\ norm} = I_i \times 0.6/(\text{slit width})$, $\sigma_{norm}(I_i) = \sigma(I_i) \times 0.6/(\text{slit width})$, taking into account actual value of divergence slit width which was used to measure each particular intensity I_i, and saved in xye-type file. So transformed powder pattern has usual view in whole 2θ range 9-140°, but all high-angle points have small esd's. The photoluminescence (PL) and photoluminescence excitation (PLE) spectra of the samples were analyzed by using a Spex Fluorolog-3 Spectrofluorometer equipped with a 450W Xe light source. The Commission International de l'Eclairage (CIE) chromaticity coordinates for all samples were measured by a Laiko DT-101 color analyzer equipped with a CCD detector (Laiko Co., Tokyo, Japan). Time-resolved measurements were performed with a tunable nanosecond optical-parametric-oscillator/Q-switch-pumped YAG:Nd^{3+} laser system (NT341/1/UV, Ekspla). Emission transients were collected with a nanochromater (SpectraPro-300i, ARC), detected with photomultiplier tube (R928HA, Hamamatsu), connected to a digital oscilloscope (LT372, LeCrop) and transferred to a computer for kinetics analysis. Thermal quenching measurements were investigated using a heating apparatus (THMS-600) in combination with a Jobin-Yvon Spex, Model FluoroMax-3 spectrophotometer.

2.3. Theoretical calculations

All theoretical calculations were based on density functional theory (DFT) [34,35] and all calculations were done by CASTEP packages [36] Ultrasoft pseudopotentials [37] and planewaves with cutoff energy 380 eV were implemented. In addition, revised Perdew Burke Ernzerhof (rPBE) functional [38] was used to treat electron exchange-correlation energy. The unit cell of $Ca_2Y_8(SiO_4)_6O_2$ was obtained by X-ray diffraction measurements. The structure possessed $P6_3/m$ symmetry with lattice parameters, a = 9.3507 Å, b = 9.3507 Å, c = 6.7889 Å, α = 90°, β = 90°, and γ = 120°. Sm^{3+} doped $Ca_2Y_8(SiO_4)_6O_2$was constructed by replacing one of Y^{3+} in $Ca_2Y_8Sm(SiO_4)_6O_2$ by one Sm^{3+} because their similar atomic radii and charges. We assumed Sm^{3+} was in low-spin state, and spin polarizations were considered in the theoretical calculations of $Ca_2Y_7Sm(SiO_4)_6O_2$. The geometry optimization was carried out on both systems, $Ca_2Y_8(SiO_4)_6O_2$ and $Ca_2Y_7Sm(SiO_4)_6O_2$ without any symmetry constraint. The Monkhorst-pack mesh was set 1 × 1 x 2 for geometry optimizations and 2 × 2 x 2 for density of state (DOS) and projected density of state (PDOS) calculations. The optimization criteria for energy, max forces, max stress, and max displacements were 1.0×10^{-5} eV/atom, 0.03 eV/Å, 0.05 GPa, and 0.001 Å respectively. The tolerance of self-consistent field calculations (SCF) was 2.0×10^{-6} eV/atom.

3. Results and discussion

3.1. Crystal structure

For the purpose of investigating the phase purity, crystal structure and crystallinity of as-synthesized powders, X-ray diffraction patterns were measured. Fig. 1(a) shows the XRD pattern of $Ca_2Y_8(SiO_4)_6O_2$:$0.01Sm^{3+}$ phosphors as well as the standard pattern for $Ca_2Y_8(SiO_4)_6O_2$ (ICSD file no.252709) as reference. It revealed that all the diffraction peaks of the as-prepared powders are consistent with the Standard pattern (ICSD file no.252709). There are no any impurity and second phase. Therefore, the results illustrate that the samples are single phase and the host will not be changed even though which are doped with Sm^{3+} ions. $Ca_2Y_8(SiO_4)_6O_2$ crystallizes as a hexagonal system with the space group $P6_3/m$, whose lattice parameters are a = 9.3057 Å, b = 9.3057 Å. c = 6.7899 Å, α = 90°, β = 90°, γ = 120°, and Z = 1. Fig. 2 presents the $Ca_2Y_8(SiO_4)_6O_2$ structure and coordination of Y ion. As shown in Fig. 2, Y ion is coordinated by four and nine oxygen. The ionic radii of six-coordinated and nine-coordinated Y^{3+} ions are 0.90 Å and 1.08 Å, respectively. The ionic radii of six-coordinated and nine-coordinated Sm^{3+} ions are 0.96 Å and 1.13 Å, respectively. Therefore, the Sm^{3+} ions are expected to substitute Y^{3+} ions due to the similar ionic radii and charge valences.

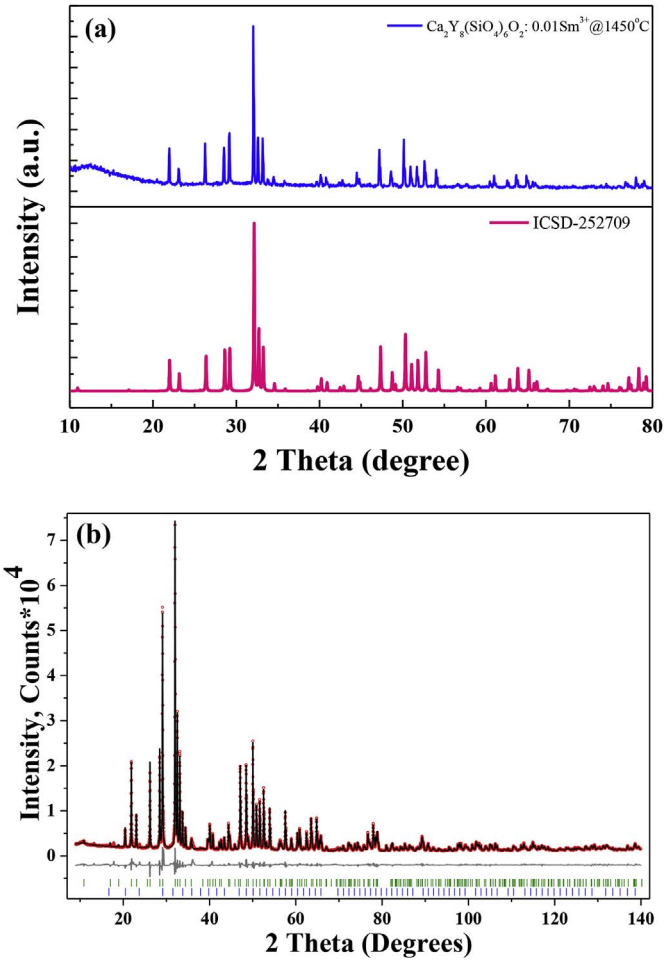

Fig. 1. (a) Powder XRD patterns of $Ca_2Y_8(SiO_4)_6O_2$:0.01Sm^{3+}. ($Ca_2Y_8(SiO_4)_6O_2$ file no. ICSD: 252709). (b) Difference Rietveld plot of $Ca_2Y_8(SiO_4)_6O_2$:0.01Sm^{3+}.

Moreover, this structure exhibits one crystallography nonequivalent site of cation, that is 4f site with nine-coordinated [Ca^{2+}/Y^{3+}]. The occupancy of Ca^{2+} and Y^{3+} in the 4f site are 49.9% and 50.1%. In order to further comprehend the $Ca_2Y_8(SiO_4)_6O_2$ structure, the structure was refined by the Rietveld refinement method.

3.2. Rietveld refinement

Rietveld refinement was performed by using TOPAS 4.2 [39] which accounts esd's of each point by special weight scheme. Almost all peaks besides small amount of Y_2O_3 impurity peaks indexed by hexagonal cell ($P6_3/m$) with parameters close to $Ca_2Y_8(SiO_4)_6O_2$:Bi^{3+} [40], therefore this crystal structure was taken as starting model for Rietveld refinement. There are two Ca/Y sites in the asymmetric part of unit cell, and occupations of Ca^{2+} and Y^{3+} ions in both of them were refined with linear restriction occ(Ca) + occ(Y) = 1 for each site. The Sm^{3+} ions were not accounted in refinement due to small concentration value. All thermal parameters of ions were refined isotropically. Refinement was stable and gives low *R*-factors (Table 1, Fig. 2). Coordinates of atoms and main bond lengths are in Table 2 and Table 3, respectively. Chemical formula after refinement was $Ca_{2.94(6)}Y_{7.06(6)}(SiO_4)_6O_2$, which is only slightly differ from expected one $Ca_2Y_8(SiO_4)_6O_2$.

3.3. Luminescence properties

Fig. 3(a) shows the PLE spectra of $Ca_2Y_8(SiO_4)_6O_2$:Sm^{3+} phosphors. The strongest peak of excitation is located at 405 nm monitored at 601 nm emission, which is ascribed to $^6H_{5/2} \rightarrow {}^4F_{7/2}$ transition of Sm^{3+}

Table 1
Main parameters of processing and refinement of the $Ca_2Y_8(SiO_4)_6O_2$:0.01Sm^{3+} sample.

Compound	$Ca_2Y_8(SiO_4)_6O_2$:0.01Sm^{3+}
Sp.Gr.	$P6_3/m$
a, Å	9.3549 (2)
c, Å	6.7879 (1)
V, Å^3	514.45 (2)
Z	1
2*θ*-interval, °	9–140
R_{wp}, %	5.02
R_p, %	4.00
R_{exp}, %	1.48
χ^2	3.39
R_B, %	1.46

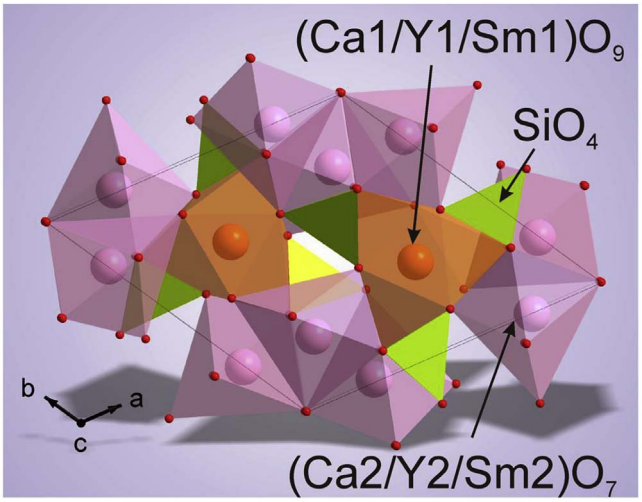

Fig. 2. The crystal structure of $Ca_2Y_8(SiO_4)_6O_2$ and coordination sphere of Y ion.

Table 2
Fractional atomic coordinates and isotropic displacement parameters (Å^2) of $Ca_2Y_8(SiO_4)_6O_2$:0.01Sm^{3+}.

	x	*y*	*z*	B_{iso}	Occ.
Ca1	1/3	2/3	−0.0019 (4)	1.29 (5)	0.479 (7)
Y1	1/3	2/3	−0.0019 (4)	1.29 (5)	0.521 (7)
Ca2	0.2377 (1)	0.0038 (2)	0.25	0.87 (4)	0.171 (9)
Y2	0.2377 (1)	0.0038 (2)	0.25	0.87 (4)	0.829 (9)
Si1	0.3720 (3)	0.3993 (3)	0.25	1.04 (7)	1
O1	0.2462 (5)	0.3378 (5)	0.4400 (5)	2.2 (1)	1
O2	0.4815 (7)	0.3106 (7)	0.25	2.0 (1)	1
O3	0.5276 (8)	0.3979 (8)	0.75	2.4 (2)	1
O4	0	0	0.25	3.2 (2)	1

Table 3
Main bond lengths (Å) of $Ca_2Y_8(SiO_4)_6O_2$:0.01Sm^{3+}.

(Ca1/Y1)—O1^{i}	2.793 (4)	(Ca2/Y2)—O3^{v}	2.382 (5)
(Ca1/Y1)—O2^{ii}	2.348 (4)	(Ca2/Y2)—O4	2.206 (1)
(Ca1/Y1)—O3^{iii}	2.402 (5)	Si1—O1	1.644 (3)
(Ca2/Y2)—O1^{iv}	2.409 (4)	Si1—O2	1.609 (4)
(Ca2/Y2)—O1^{v}	2.282 (4)	Si1—O3^{iii}	1.643 (7)
(Ca2/Y2)—O2	2.626 (6)		

Symmetry codes: (i) -*x* + *y*, -*x*+1, -*z*+1/2; (ii) -*x*+1, -*y*+1, -*z*; (iii) -*x*+1, -*y*+1, -*z*+1; (iv) -*x* + *y*, -*x*, -*z*+1/2; (v) *y*, -*x* + *y*, -*z*+1.

The excitation spectra include a series of peaks, which arise at 361, 377, 405 and 475 nm, which are attributed to $^6H_{5/2} \rightarrow {}^4D_{3/2}$, $^6H_{5/2} \rightarrow {}^4D_{7/2}$, $^6H_{5/2} \rightarrow {}^4F_{7/2}$, $^6H_{5/2} \rightarrow {}^4I_{13/2}$ transition, respectively. Fig. 3(b) shows the emission spectra of $Ca_2Y_8(SiO_4)_6O_2$:Sm^{3+} phosphors. Upon 405 nm

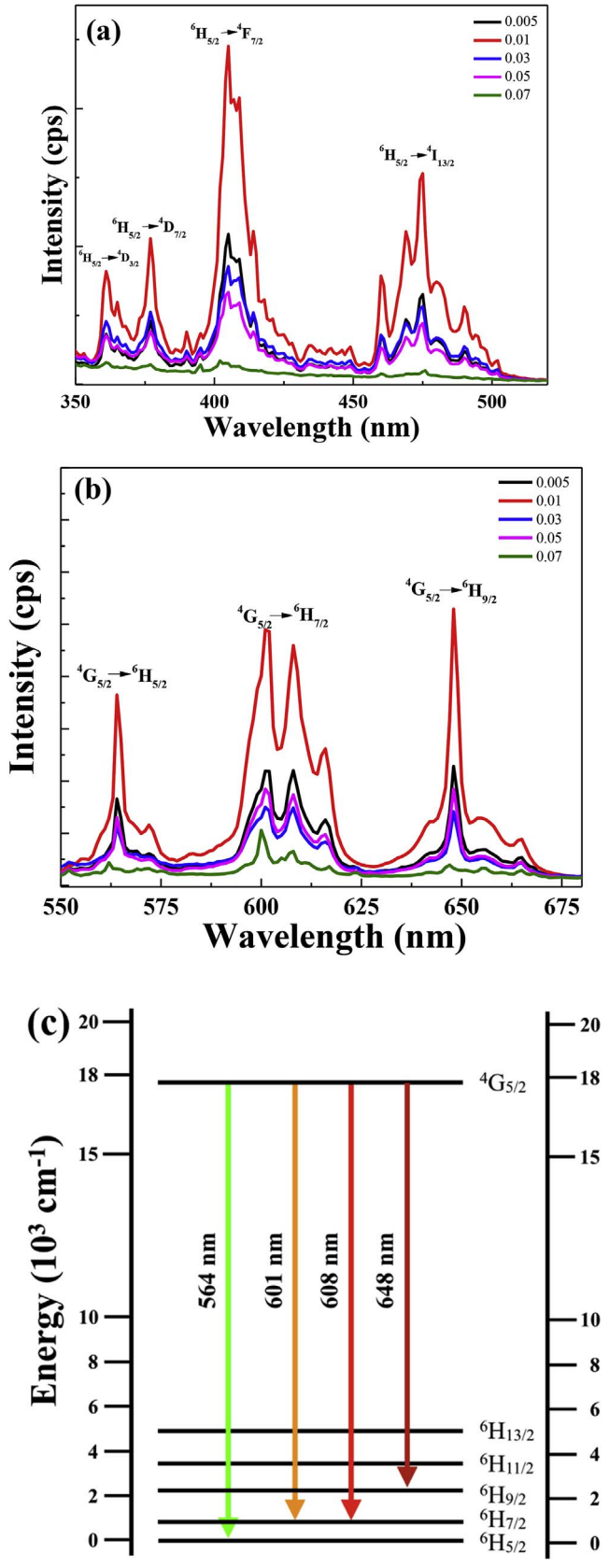

Fig. 3. (a) The PLE spectra of $Ca_2Y_8(SiO_4)_6O_2$:*x* mol.% Sm^{3+} phosphors (*x* = 0.5–7) monitored at 601 nm; (b) The PL spectra of $Ca_2Y_8(SiO_4)_6O_2$:*x* mol.% Sm^{3+} phosphors (*x* = 0.5–7) excited at 405 nm; (c) Energy level diagram of Sm^{3+} shows the in $Ca_2Y_8(SiO_4)_6O_2$ phosphors.

excitation, the PL spectra present several emission peaks located at 564, 601, 608 and 648 nm, which can be ascribed to the transition of $^4G_{5/2} \rightarrow {}^6H_{5/2}$, $^4G_{5/2} \rightarrow {}^6H_{7/2}$, $^4G_{5/2} \rightarrow {}^6H_{7/2}$ and $^4G_{5/2} \rightarrow {}^6H_{9/2}$, respectively. The intensity of luminescence increased as the concentration of Sm^{3+} increased and the optimal doped concentration was found to be 1 mol.%. This situation is due to concentration quenching, which is resulted from two mechanisms in a compound. One is exchange interaction, and the other is multipolar interaction [41]. As increasing the content of activators, the distances between activators will become shorter. Therefore, the non-radiative energy transfer between the nearest-neighbor activators leads to the re-absorption of radiation and decreases the intensity of emission.

In this study, we calculated the values of the critical distance (R_c) through both concentration quenching method and spectral overlap method. For the purpose of clarifying which mechanism is responsible for the concentration quenching effect. Therefore, we calculated the critical energy transfer distance (R_C) through the following equation proposed by Blasse [42–45]:

$$Rc \approx 2\left[\frac{3V}{4\pi X_c N}\right]^{1/3} \quad (1)$$

where *V* presents the volume of unit cell, *Xc* stands for the critical concentration of Sm^{3+} ions and *N* is the number of cations in the unit cell. For $Ca_2Y_8(SiO_4)_6O_2$ host, $V = 514.14$ Å^3, $Xc = 0.01$ and $N = 1$. Consequently, the critical distance (R_c) is calculated to be 46.13 Å. For the electric dipole-dipole interaction, the critical distance (R_c) for the energy transfer can be expressed by:

$$R_c^6 = 0.63 \times 10^{28}\frac{Q_A}{E_s^4}\int F_s(E)F_A(E)dE \quad (2)$$

where $Q_A = 4.8 \times 10^{-16} f_d$ is the absorption cross section of Sm^{3+}, $f_d \approx 0.34$ is the electric dipole oscillator strength for Sm^{3+} ions, and E_s in (eV) is the maximum energy of spectral overlap. $\int F_s(E)F_A(E)dE$ represents the spectral overlap between the normalized spectra shapes of emission $F_s(E)$ and excitation $F_A(E)$. Therefore, the critical distance is calculated to be 55 Å by spectral overlap method, which is approximately consistent with that obtained by concentration method. According to the presented work, the possibility of exchange interaction was excluded because it only takes place when the critical distance is less than 5 Å [46].

The probability of energy transfer between the activator ions can be calculated by the following equation [47–49]:

$$\frac{I}{x} = \frac{k}{1+\beta(x)^{\theta/3}} \quad (3)$$

where I is the emission intensity, *x* stands for the concentration of activator. *k* and β are constants for the same host under the same excitation condition. The kinds of non-radiative can be explained by the values of θ. The value of θis 6, 8, and 10 corresponding to dipole-dipole (d-d), dipole-quadrupole (d-q), quadrupole-quadrupole interactions (q-q), respectively. The relationship between log (I/x) and log(x) is shown in Fig. 4 The slope of the linear fit is (-θ/3), which was calculated to be -1.4. Therefore, the value of θ is approximately estimated to be 6. Therefore, the result illustrates that the main type of energy transfer is dipole-dipole interaction.

The temperature-dependence luminescence intensity is an essential property for high power LED application. Fig. 5(a) shows the temperature-dependence luminescence intensity as a function of temperature for $Ca_2Y_8(SiO_4)_6O_2$: 1 mol.% Sm^{3+} phosphor excited at 405 nm. The PL intensity of the four emission peaks located at 564, 601, 608 and 648 nm were attributed to the transitions of $^4G_{5/2} \rightarrow {}^6H_{5/2}$, $^4G_{5/2} \rightarrow {}^6H_{7/2}$, $^4G_{5/2} \rightarrow {}^6H_{7/2}$ and $^4G_{5/2} \rightarrow {}^6H_{9/2}$, respectively. It was investigated that increasing the temperature from 25 °C to 300 °C would lead to the decrease of these transitions. Fig. 5(a) illustrated that the temperature-dependence luminescence intensity of $Ca_2Y_8(SiO_4)_6O_2$:0.01Sm^{3+} was decreased to

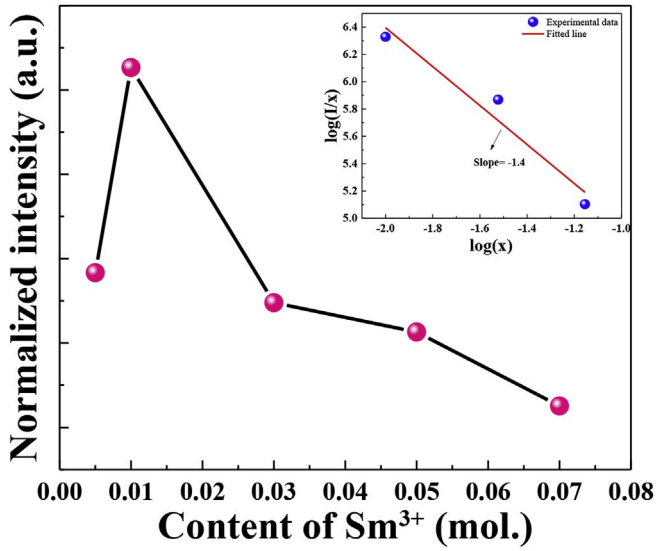

Fig. 4. The concentration quenching of $Ca_2Y_8(SiO_4)_6O_2:Sm^{3+}$ under 405 nm excitation. The inset plot shows the relationship of log (x) vs log (I/x).

94%, 86%, 80%, 72%, 66%, and 58% at 50, 100, 150, 200, 250 and 300 °C, respectively. These results indicated that $Ca_2Y_8(SiO_4)_6O_2:0.01Sm^{3+}$ phosphors exhibit an excellent thermal stability. It is believed that the intensity decreases as the temperature increase due to the thermal quenching effect. To the best of our knowledge, thermal quenching is due to the nonradiative relaxation process through the intersection point between the ground state and excited state as depicted in Fig. 5(c) [50,51]. Fig. 5(b) demonstrates the activation energy (E_a) of $Ca_2Y_8(SiO_4)_6O_2:0.01Sm^{3+}$ phosphor. The activation energy (E_a) can be expressed by Ref. [52]:

$$\ln\left(\frac{I_0}{I}\right) = \ln A - \frac{E_a}{k_B T} \quad (4)$$

where I_0 and I stand for the luminescence intensity of the $Ca_2Y_8(SiO_4)_6O_2:0.01Sm^{3+}$ phosphor at room temperature and the measuring temperature (25–300 °C), respectively, A is a constant, and k_B is the Boltzmann constant (8.617×10^{-5} eV/K). The E_a was calculated to be 0.16 eV.

The diffuse reflection spectra of undoped and Sm^{3+}-doped $Ca_2Y_8(SiO_4)_6O_2$ host is depicted as Fig. 6 The undoped host presents the strongest absorption around 400 nm region. As the Sm^{3+} ions are doped into the host, the DR spectra show the several absorption peaks from 360 to 500 nm. Those can be ascribed to the absorption of $^6H_{5/2} \rightarrow {}^4D_{3/2}$, $^6H_{5/2} \rightarrow {}^4D_{7/2}$, $^6H_{5/2} \rightarrow {}^4F_{7/2}$, $^6H_{5/2} \rightarrow {}^4I_{13/2}$ transition of Sm^{3+}, which are consistent well with the excitation spectra. The band gap of the host can be estimated by the following formula [1,53]:

$$[F(R_\infty)hv]^n = A(hv - E_g) \quad (5)$$

where hv is the photon energy, A is proportional constant and E_g is the energy of band gap, n = 1/2, 2, 3, 3/2 for direct, indirect allowed transition and forbidden transition, respectively. $F(R_\infty)$ is the Kubelka-Munk function denoted as:

$$F(R_\infty) = (1 - R)^2 / 2R = K/S \quad (6)$$

It is well known that the lifetime plays an important role for the application of light source and display technology. The PL intensity is proportional to radiative transition probability and the lifetime is the reciprocal of the sum of radiative transition, non-radiative transition and energy transfer probability [54]. To obtain the better comprehension of energy transfer process, the decay curves are presented in Fig. 7. It exhibits the typical decay curves of Sm^{3+} $^6H_{5/2} \rightarrow {}^4F_{7/2}$ emission centered at 601 nm upon excitation at 403 nm. The decay curves were well fitted with a second-order exponential decay mode by the

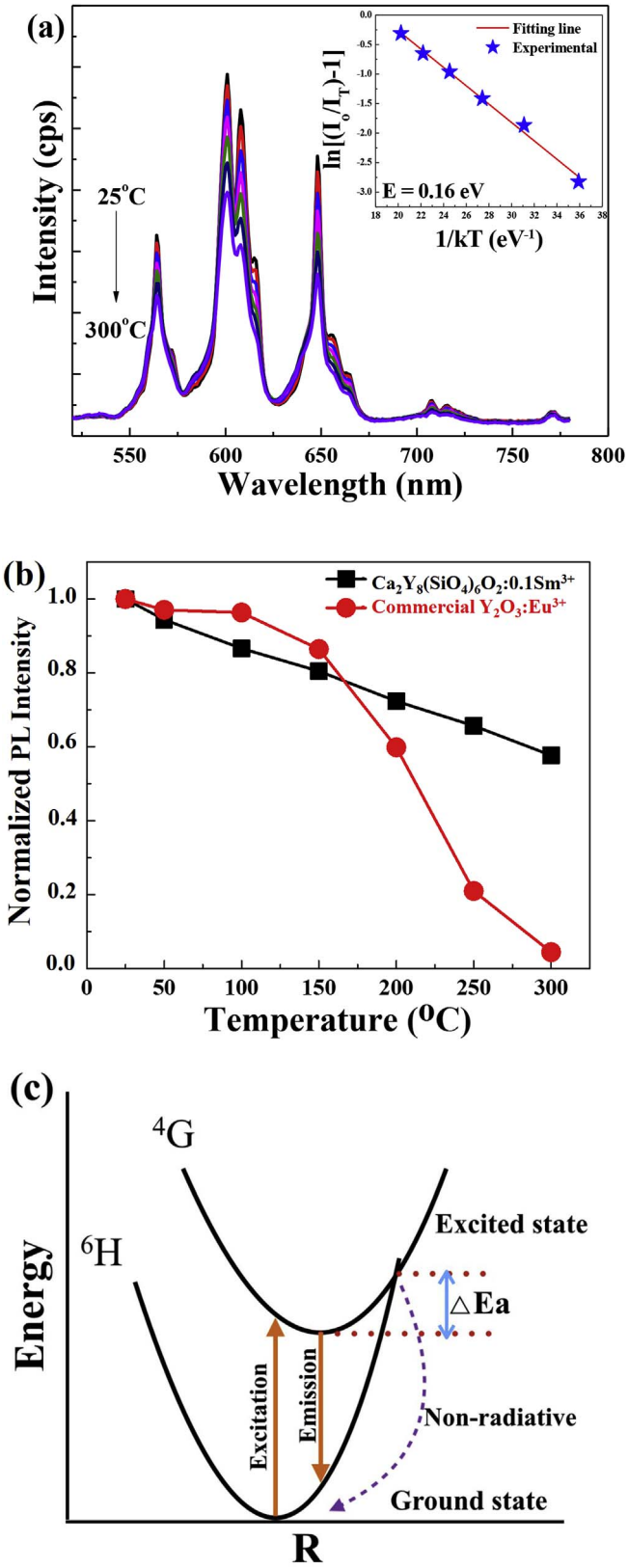

Fig. 5. (a)The Temperature dependence of the PL intensity $Ca_2Y_8(SiO_4)_6O_2$:1 mol.% Sm^{3+} phosphor. (Inset: The relationship between activation energy (*Ea*) and inverse temperature (1/T); (b) Comparison of thermal stability for commercial red-emitting phosphor-$Y_2O_3:Eu^{3+}$ and as-synthesized $Ca_2Y_8(SiO_4)_6O_2$:1 mol.% Sm^{3+} phosphor; (c) Configurational coordinate diagram that shows the thermal quenching process of $Ca_2Y_8(SiO_4)_6O_2:Sm^{3+}$.

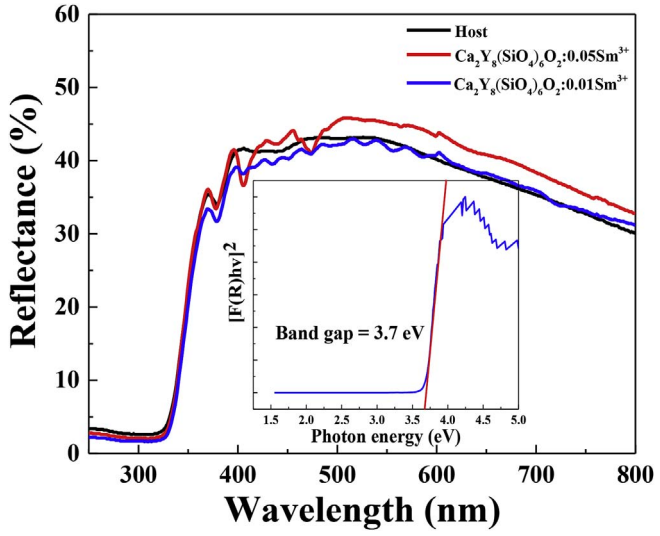

Fig. 6. The diffuse reflection spectra of undoped and Sm^{3+}-doped $Ca_2Y_8(SiO_4)_6O_2$. Inset: linear extrapolation of the energy of band gap for $Ca_2Y_8(SiO_4)_6O_2$ host.

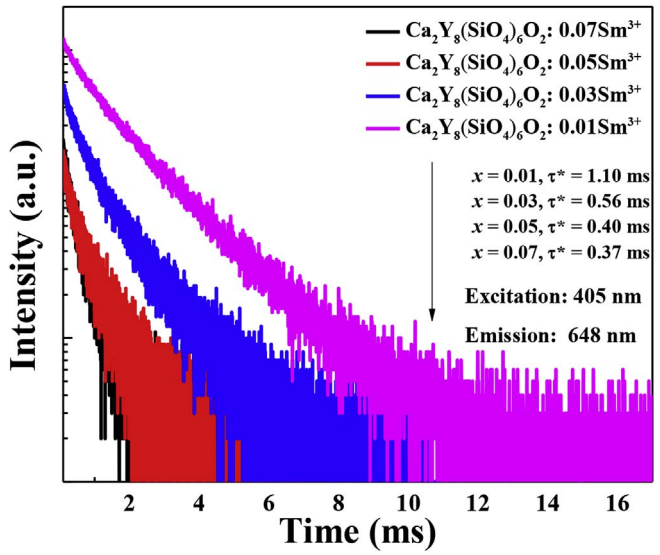

Fig. 7. Decay curves of Sm^{3+} emission monitored at 601 nm for $Ca_2Y_8(SiO_4)_6O_2$:xSm^{3+} phosphors (x = 0.01–0.07) under excitation at 405 nm.

following equation [55]:

$$I = A_1 \exp\left(-\frac{t}{\tau_1}\right) + A_2 \exp\left(-\frac{t}{\tau_2}\right) \quad (7)$$

where I is the luminescence intensity; A_1 and A_2 are constants; t is the time, and τ_1 and τ_2 are short- and long-lifetimes for exponential components, respectively. Using these parameters, the average decay times τ^* can be determined by the formula as follows [56,57]:

$$\tau^* = (A_1\tau_1^2 + A_2\tau_2^2)/(A_1\tau_1 + A_2\tau_2) \quad (8)$$

The average decay times τ^* were determined to be 1.10, 0.56, 0.4, and 0.37 ms for $Ca_2Y_8(SiO_4)_6O_2$: xSm^{3+} phosphors with x = 0.01, 0.03, 0.05, and 0.07, which was in fairly good agreement to those values reported in the literature.

For the purpose of determining the quantum efficiency (Φ) of the $Ca_2Y_8(SiO_4)_6O_2$: xSm^{3+} phosphors, it was calculated by the absorption efficiency (A) and quantum efficiency (Φ). The measurement was performed by using the barium sulfate coated integrating sphere which was attached to the spectrophotometer. The absorption efficiency (A) and quantum efficiency (Φ) can be expressed by Refs. [58,59]:

$$A = \frac{\int E_R - \int R_s}{\int E_R} \quad (9)$$

$$\Phi = \frac{\int \lambda_s}{\int E_s - \int E_R} \quad (10)$$

where A stands for the emission spectrum of the samples, E_S and E_R presents the spectra of the excitation light with and without the samples in the integrating sphere. In this case, the quantum efficiency (Φ) of $Ca_2Y_8(SiO_4)_6O_2$: xSm^{3+} phosphor was estimated to be 54%.

3.4. Band structure and density of states

The optimized cell parameters *a*, *b*, and *c* were 5% lager than experimental data, and the doping of Sm made the cell parameters *a* and *b* 0.5% larger than the undoped $Ca_2Y_8(SiO_4)_6O_2$. The minute change in cell parameters indicated that the Sm doping did not change the crystal structure much. Figs. 8 and 9 showed the bandgaps, DOS, and PDOS of $Ca_2Y_8(SiO_4)_6O_2$ and Ca_2Y_7Sm $(SiO_4)_6O_2$. The band gap of $Ca_2Y_8(SiO_4)_6O_2$ was 4.1 eV at the gamma point of the Brillouin zone. The differences between the calculated and experimentally measured band gaps may have various reasons. As the computational models had some constrains, which made it deviate from the actual situation. The possible reasons are: i) the amount of Sm^{3+} ions, which were significantly higher in the computational model. ii) XRD measurements shown that there were statistic distributions of Ca and Y in the Y1 and Y2 sites. The small simulation cell used in this study was not able to capture this geometrical feature. In addition, the Sm^{3+} ions could occupy Y1 or Y2 sites, and simulation studies cannot test all possible structures by the limited cell size. The VBM and CBM were mainly composed of 2p bands of oxygen atoms and 4d bands of yttrium atoms respectively. After doping samarium, localized states appeared between VBM and CBM. These localized states were 1.3–2.3 eV lower than CBM and there was also a localized state very close to Fermi level. These localized states were composed of 4f states of doped samarium atoms. Under ultraviolet radiation, the electrons excited either from VBM to CBM or these localized states. Therefore, the charge excitation occurred from 2p bands of oxygen atoms to 4f states of samarium atoms forming charge transfer bands (CTB). Because the localized states were in the forbidden band, the Sm 4f-4f transition took place easily leading to a series of excitation bands from 350 to 500 nm.

3.5. Fabrication

The EL spectra of fabricated LEDs driven by various currents from 40 mA to 150 mA were shown in Fig. 10. The white-light LED was fabricated with commercial phosphors: $BaMgAl_{10}O_{17}:Eu^{2+}$ (BAM), $(Ba,Sr)_2SiO_4:Eu^{2+}$ and as-synthesized CYSO:0.01Sm^{3+} phosphors. The CIE coordinates of W-LEDs illuminated under 40, 60, 80, 150 *m*A were (0.265, 0.280), (0.260, 0.287), (0.261, 0.288), and (0.267, 0.289) as shown in inset of Fig. 10. Furthermore, the CRI and CCT of the fabricated w-LED driven by 150 *m*A currents was determined to be 75 and 11357 K. It could be suggested that the samples are very stable under various currents due to of the slight moving on CIE coordinate system.

4. Conclusions

In summary, we report novel red-emitting $Ca_2Y_8(SiO_4)_6O_2$:Sm^{3+} phosphors by a solid-state method and investigate their crystal structure, luminescence properties, decay curves as well as thermal quenching and LED fabrications. The phosphor shows excitation spectrum with a broad band and several sharp bands in 350–500 nm region. The emission spectra show an intense and high color purity red emission at 601 nm with CIE chromaticity coordinates of (0.569, 0.363). The luminescence decay lifetime of $Ca_2Y_8(SiO_4)_6O_2$:xSm^{3+} phosphors were measured to be 1.10–0.37 ms. The thermal stability test indicated

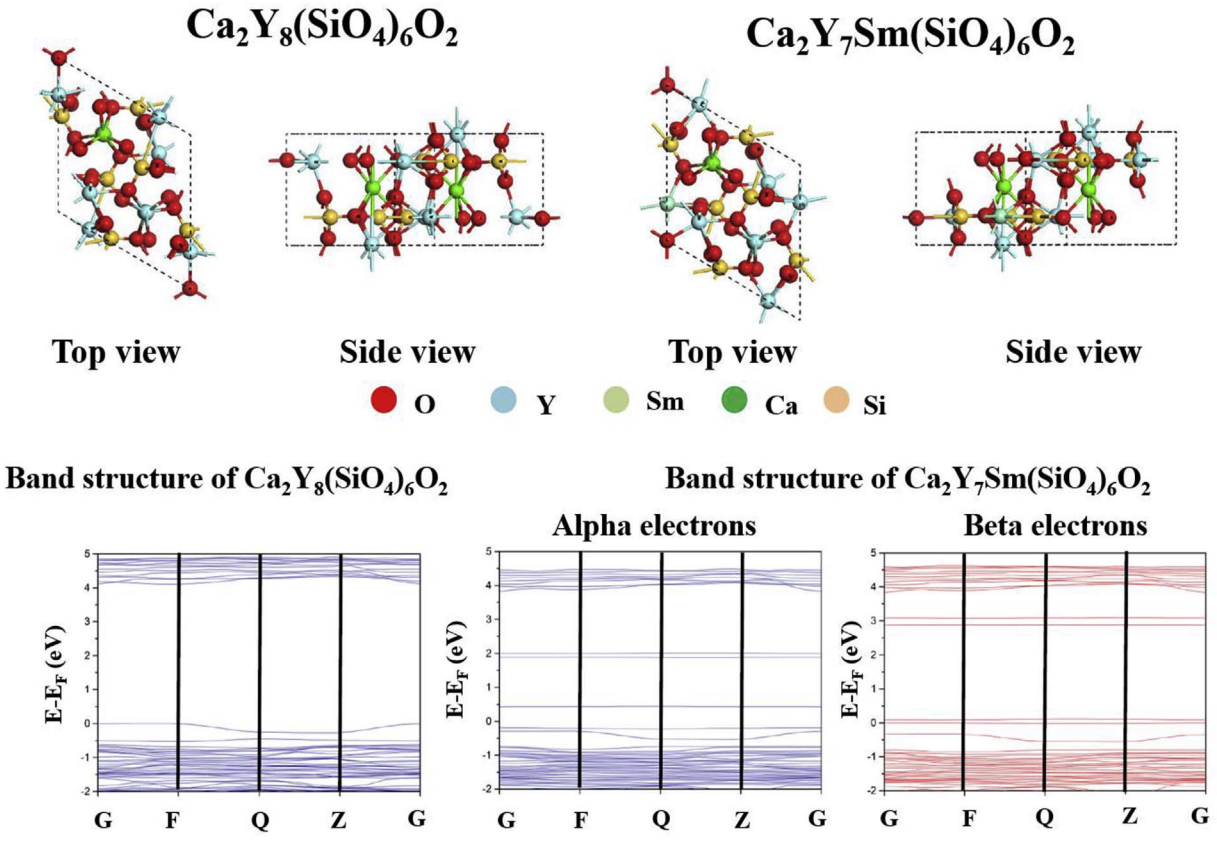

Fig. 8. The models and band structures of undoped $Ca_2Y_8(SiO_4)_6O_2$ supercell and $Ca_2Y_8(SiO_4)_6O_2:Sm^{3+}$ supercell with one Sm atom substituting Y.

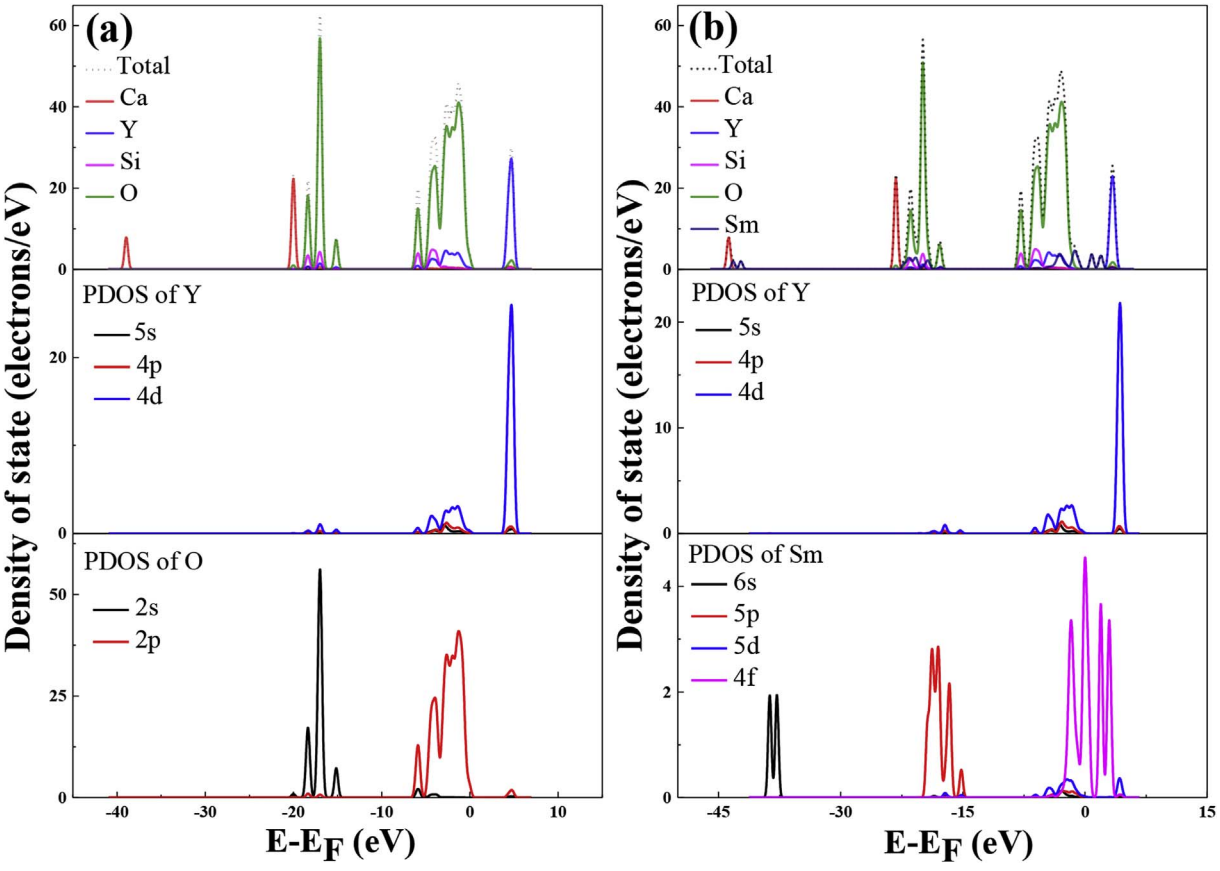

Fig. 9. (a) The total and partial density of state for $Ca_2Y_8(SiO_4)_6O_2$ host; (b) The total and partial density of state for $Ca_2Y_7Sm(SiO_4)_6O_2$ phosphors.

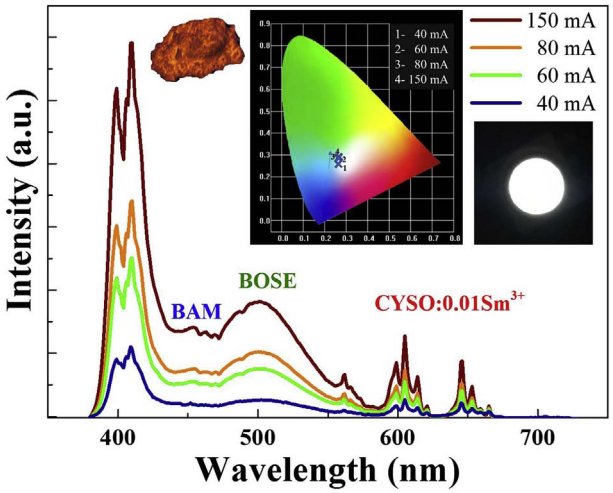

Fig. 10. The electroluminescence of the w-LED driven by the current from 40 to 150 *m*A. Inset: photos CYSO:Sm^{3+} phosphor excited in UV box, fabricated w-LED and the CIE coordinates of various current of the fabricated W-LED.

that the luminescence decay of 16% at 150 °C and the activation energy E_a was calculated to be 0.16 eV by thermal quenching. The band structure and density of state for both $Ca_2Y_8(SiO_4)_6O_2$ and $Ca_2Y_7Sm(SiO_4)_6O_2$ calculated by first principles calculations are in well consistent with our experimental data. We believe CYSO:Sm^{3+} could be a potential blue-excitable and red-emitting phosphor for light emitting diodes.

Acknowledgment

This research was supported by Minister of Science and Technology under contract no. MOST 105-2622-E-033-003-CC2 and MOST 104-2628-E-033-002-MY3.

Appendix A. Supplementary data

Supplementary data related to this article can be found at http://dx.doi.org/10.1016/j.dyepig.2017.10.047.

References

[1] Ding X, Zhu G, Geng W, Wang Q, Wang Y. Rare-earth-free high-efficiency narrow-band red-emitting $Mg_3Ga_2GeO_8:Mn^{4+}$ phosphor excited by near-UV light for white-light-emitting diodes. Inorg Chem 2015;55(1):154–62.
[2] Zhang S, Hu Y, Duan H, Fu Y, He M. An efficient, broad-band red-emitting $Li_2MgTi_3O_8:Mn^{4+}$ phosphor for blue-converted white LEDs. J Alloys Compd 2017;693:315–25.
[3] Liang S, Shang M, Lian H, Li K, Zhang Y, Lin J. Deep red $MGe_4O_9:Mn^{4+}$(M= Sr, Ba) phosphors: structure, luminescence properties and application in warm white light emitting diodes. J Mater Chem C 2016;4(26):6409–16.
[4] Cao R, Luo W, Xiong Q, Liang A, Jiang S, Xu Y. Synthesis and luminescence properties of novel red phosphors $LiRGe_2O_6:Mn^{4+}$(R = Al or Ga). J Alloys Compd 2015;648:937–41.
[5] Li J, Yan H, Yan F. Synthesis and luminescence characterization of a new yellowish-orange phosphor: $Ba_2B_{10}O_{17}:Sm^{3+}$. Luminescence 2017;32(1):30–4.
[6] Zhang Y, Li X, Li K, Lian H, Shang M, Lin J. Crystal-site engineering control for the reduction of Eu^{3+} to Eu^{2+} in $CaYAlO_4$: structure refinement and tunable emission properties. ACS Appl Mater interfaces 2015;7(4):2715–25.
[7] Mickens MA, Assefa Z. Tunable luminescence and white light emission of novel multiphase sodium calcium silicate nanophosphors doped with Ce^{3+}, Tb^{3+}, and Mn^{2+} ions. J Luminescence 2014;145:498–506.
[8] Nair GB, Dhoble S. Orange light-emitting $Ca_3Mg_3(PO_4)_4:Sm^{3+}$ phosphors. Luminescence 2017;32(1):125–8.
[9] Wu L, Bai Y, Wu L, Yi H, Kong Y, Zhang Y, et al. Sm^{3+} and Eu^{3+} codoped $SrBi_2B_2O_7$: a red-emitting phosphor with improved thermal stability. RSC Adv 2017;7(2):1146–53.
[10] Nagaraja R, Manjari VP, Sailaja B, Ravikumar R. A novel orange emitting Sm^{3+} ions doped $NaCaAlPO_4F_3$ phosphor: optical and luminescence properties. J Mol Struct 2017;1130:96–102.
[11] Ju Z-H, Wei R-P, Ma J-X, Pang C-R, Liu W-S. A novel orange emissive phosphor $SrWO_4:Sm^{3+}$ for white light-emitting diodes. J Alloys Compd 2010;507(1):133–6.
[12] Mu J, Liu L, Kang S-Z. Enhancement of Sm^{3+} emission by SnO_2 nanocrystals in the silica matrix. Nanoscale Res Lett 2007;2(2):100–3.
[13] Xia Z, Chen D. Synthesis and luminescence properties of $BaMoO_4:Sm^{3+}$ phosphors. J Am Ceram Soc 2010;93(5):1397–401.
[14] Zhang Y, Ran P, Chengyu L, Chunyu Z, Qiang S. Reddish orange long lasting phosphorescence of Sm^{3+} in $Sr_2ZnSi_2O_7:Sm^{3+}$ phosphors. J Rare Earths 2010;28(5):705–8.
[15] Bedyal A, Kumar V, Ntwaeaborwa O, Swart H. A promising orange-red emitting nanocrystalline $NaCaBO_3:Sm^{3+}$ phosphor for solid state lightning. Mater Res Express 2014;1(1):015006.
[16] Guo Q, Zhao C, Liao L, Lis S, Liu H, Mei L, et al. Luminescence investigations of novel orange-red fluorapatite $KLaSr_3(PO_4)_3F$: Sm^{3+} phosphors with high thermal stability. J Am Ceram Soc 2017;100(5):2221–31.
[17] Xu J, Ju Z, Gao X, An Y, Tang X, Liu W. $Na_2CaSn_2Ge_3O_{12}$: a novel host lattice for Sm^{3+}-doped long-persistent phosphorescence materials emitting reddish orange light. Inorg Chem 2013;52(24):13875–81.
[18] Zou X, He L, Li R, Zheng Q, Liu Y, Xu C, et al. Structure and luminescent properties of $Ca_3Bi(PO_4)_3:Sm^{3+}$ orange phosphor. J Mater Sci Mater Electron 2017;28(3):2826–32.
[19] Manhas M, Kumar V, Singh VK, Sharma J, Prakash R, Sharma V, et al. A novel orange-red emitting $Ba_2Ca(BO_3)_2:Sm^{3+}$ phosphor to fill the amber gap in LEDs: synthesis, structural and luminescence characterizations. Curr Appl Phys 2017;17(11):1369–75.
[20] Li G, Wei Y, Long W, Xu G. Photoluminescence properties, energy transfer and thermal stability of the novel red-emitting $CaGd_2(WO_4)_4:Eu^{3+}$, Sm^{3+} phosphors. Mater Res Bull 2017;95:86–94.
[21] Min X, Huang Z, Fang M, Liu Y-G, Tang C, Wu X. Energy transfer from Sm^{3+} to Eu^{3+} in red-emitting phosphor $LaMgAl_{11}O_{19}$: Sm^{3+}, Eu^{3+} for solar cells and near-ultraviolet white light-emitting diodes. Inorg Chem 2014;53(12):6060–5.
[22] Sun JY, Cui DP, Di QM, Xu QG, Han L. Photoluminescence and energy transfer from Sm^{3+} to Eu^{3+} in $Na_3YSi_2O_7$ phosphor for light-emitting diodes. Proc Appl Mech Mater Trans Tech Publ 2014:117–20.
[23] Lu G, Qiu K, Li J, Zhang W, Yuan X. Synthesis and photoluminescence characteristics of Sm^{3+}-doped $Bi_4Si_3O_{12}$ red-emitting phosphor. Luminescence 2017;32(1):93–9.
[24] Gokhe U, Koparkar K, Omanwar S. Synthesis and photoluminescence properties of near-UV pumped novel Sm^{3+} doped β-$LiAlSiO_4$ phosphor for red-orange LEDs. J Alloys Compd 2016;689:992–7.
[25] Kang D, Yoo HS, Jung SH, Kim H, Jeon DY. Synthesis and photoluminescence properties of a novel red-emitting $Na_2Y_2Ti_3O_{10}:Eu^{3+}$, Sm^{3+} phosphor for white-light-emitting diodes. J Phys Chem C 2011;115(49):24334–40.
[26] Liu Y, Wang Z, Zhong J, Pan F, Liang H, Xiao Z. Synthesis and photoluminescence properties of red-emitting phosphors $Ba_2Gd_8(SiO_4)_6O_2:Eu^{3+}$. Mater Lett 2014;129:130–3.
[27] Zhou L, Yan B. In-situ sol–gel synthesis of nanophosphors $M_2Y_8(SiO_4)_6O_2:Eu^{3+}$ (M= Ca, Sr) derived from novel crosslinking reagents as silicon sources. J Nanosci Nanotechnol 2008;8(3):1261–5.
[28] Li G, Geng D, Shang M, Zhang Y, Peng C, Cheng Z, et al. Color tuning luminescence of $Ce^{3+}/Mn^{2+}/Tb^{3+}$-triactivated $Mg_2Y_8(SiO_4)_6O_2$ via energy transfer: potential single-phase white-light-emitting phosphors. J Phys Chem C 2011;115(44):21882–92.
[29] Sokolnicki J, Zych E. Synthesis and spectroscopic investigations of $Sr_2Y_8(SiO_4)_6O_2:Eu^{2+}$, Eu^{3+} phosphor for white LEDs. J Luminescence 2015;158:65–9.
[30] Jun L, Qiang S. A study of site occupation of Eu^{3+} in $Me_2Y_8(SiO_4)_6O_2$ (Me= Mg, Ca, Sr). Mater Chem Phys 1994;38(1):98–101.
[31] Xiumei H, Jun L, Zhe L, Xiwei Q, Mingya L, Xiaoqiang W. Photoluminescent properties of $Ca_2Gd_8(SiO_4)_6O_2:Dy^{3+}$ phosphor films prepared by sol-gel process. J Rare Earths 2008;26(6):904–6.
[32] Zhou L, Yan B. Sol–gel synthesis and photoluminescence of $M_2Gd_8(SiO_4)_6O_2:RE^{3+}$ (M= Ca, Sr; RE= Tb, Eu) phosphors by different silicate sources. J Mater Sci Mater Electron 2013;24(4):1168–74.
[33] Seeta Rama Raju G, Yu JS, Park JY, Jung HC, Moon BK. Photoluminescence and cathodoluminescence properties of nanocrystalline $Ca_2Gd_8Si_6O_{26}:Sm^{3+}$ phosphors. J Am Ceram Soc 2012;95(1):238–42.
[34] Hohenberg P, Kohn W. Inhomogeneous electron gas. Phys Rev 1964;136(3B):B864–71.
[35] Kohn W, Sham LJ. Self-consistent equations including exchange and correlation effects. Phys Rev 1965;140(4A):A1133–8.
[36] Clark Stewart J, Segall Matthew D, Pickard Chris J, Hasnip Phil J, Probert Matt IJ, Refson K, et al. First principles methods using CASTEP. Z fuer Kristallogr 2005:567.
[37] Vanderbilt D. Soft self-consistent pseudopotentials in a generalized eigenvalue formalism. Phys Rev B 1990;41(11):7892–5.
[38] Hammer B, Hansen LB, Nørskov JK. Improved adsorption energetics within density-functional theory using revised Perdew-Burke-Ernzerhof functionals. Phys Rev B 1999;59(11):7413–21.
[39] Bruker AXS. V4: general profile and structure analysis software for powder diffraction data–User's Manual. Karlsruhe, Germany: Bruker AXS; 2008. p. 2002.
[40] Sun Z, Wang M, Yang Z, Liu K, Zhu F. Crystal structure and luminescence properties of Bi^{3+} activated $Ca_2Y_8(SiO_4)_6O_2$ phosphors under near UV excitation. J Solid State Chem 2016;239:165–9.
[41] Xia Y, Liu Y-g, Huang Z, Fang M, Molokeev MS, Mei L. $Ca_6La_4(SiO_4)_2(PO_4)_4O_2:Eu^{2+}$: a novel apatite green-emitting phosphor for near-ultraviolet excited w-LEDs. J Mater Chem C 2016;4(21):4675–83.
[42] Guan A, Zhou L, Wang G, Gao F, Wang Q, Chen X, et al. Photoluminescence characterization and energy transfer of color-tunable $Li_6Y(BO_3)_3:Ce^{3+}$, Tb^{3+}

phosphors. Phys B Condens Matter 2016;494:75–81.
[43] Arunkumar P, Kim YH, Im WB. Versatile $Ca_4F_2Si_2O_7$ host from defect-induced host emission to white-light-emitting Ce^{3+}-Doped $Ca_4F_2Si_2O_7$ phosphor for near-UV solid-state lighting. J Phys Chem C 2016;120(8):4495–503.
[44] Annadurai G, Kennedy SMM, Sivakumar V. Luminescence properties of a novel green emitting $Ba_2CaZn_2Si_6O_{17}$:Eu^{2+} phosphor for white light–Emitting diodes applications. Superlattices Microstruct 2016;93:57–66.
[45] Jiao M, Guo N, Lu¨ W, Jia Y, Lv W, Zhao Q, et al. Tunable blue-green-emitting $Ba_3LaNa(PO_4)_3F$: Eu^{2+}, Tb^{3+} phosphor with energy transfer for near-UV white LEDs. Inorg Chem 2013;52(18):10340–6.
[46] Chen H, Lin H, Huang Q, Huang F, Xu J, Wang B, et al. A novel double-perovskite Gd_2ZnTiO_6:Mn^{4+} red phosphor for UV-based w-LEDs: structure and luminescence properties. J Mater Chem C 2016;4(12):2374–81.
[47] Palaspagar R, Gawande A, Sonekar R, Omanwar S. Fluorescence properties of Tb^{3+} and Sm^{3+} activated novel $LiAl_7B_4O_{17}$ host via solution combustion synthesis. Mater Res Bull 2015;72:215–9.
[48] Van Uitert L. Characterization of energy transfer interactions between rare earth ions. J Electrochem Soc 1967;114(10):1048–53.
[49] Tian Y, Feng N, Wierzbicka-Wieczorek M, Huang P, Wang L, Shi Q. Energy transfer-induced tunable emission color and thermal quenching of $Ca_3Y(PO_4)_3$:Eu^{2+}, Mn^{2+} phosphor for NUV-pumped white LEDs. Dyes Pigments 2016;131:91–9.
[50] Zhou H, Wang Q, Jiang M, Jiang X, Jin Y. A novel green-emitting phosphor $Ba_2Gd_2Si_4O_{13}$: Eu^{2+} for near UV-pumped light-emitting diodes. Dalton Trans 2015;44(31):13962–8.
[51] Fang Y-C, Chu S-Y, Kao P-C, Chuang Y-M, Zeng Z-L. Energy transfer and thermal quenching behaviors of $CaLa_2(MoO_4)_4$: Sm^{3+}, Eu^{3+} red phosphors. J Electrochem Soc 2011;158(2):J1–5.
[52] Huang C-H, Liu W-R, Chen T-M. Single-phased white-light phosphors $Ca_9Gd(PO_4)_7$:Eu^{2+}, Mn^{2+} under near-ultraviolet excitation. J Phys Chem C 2010;114(43):18698–701.
[53] Xu S, Li P, Wang Z, Li T, Bai Q, Sun J, et al. Tunable emission colors via energy transfer in $LiBaBO_3$:X (X = Ce^{3+}, Eu^{2+}, Mn^{2+}, Dy^{3+}, Sm^{3+}, Tb^{3+}) phosphors. J Mater Sci 2017;52(4):2021–34.
[54] Wang L, Moon BK, Choi BC, Kim JH, Shi J, Jeong JH. Photoluminescent properties and site occupation preference in Bi^{3+}, Eu^{3+} doped $CaY_4(SiO_4)_3O$ phosphor. Ceram Int 2016;42(11):12971–80.
[55] Pang R, Li C, Shi L, Su Q. A novel blue-emitting long-lasting proyphosphate phosphor $Sr_2P_2O_7$: Eu^{2+}, Y^{3+}. J Phys Chem Solids 2009;70(2):303–6.
[56] Ruelle N, Pham-Thi M, Fouassier C. Cathodoluminescent properties and energy transfer in red calcium sulfide phosphors (CaS: Eu, Mn). Jpn J Appl Phys 1992;31(9R):2786.
[57] Huang C-H, Chen C-T, Guo S, Zhang J-Y, Liu W-R. Luminescence and theoretical calculations of novel red-emitting $NaYPO_4F$: Eu^{3+} phosphor for LED applications. J Alloys Compd 2017;712:225–32.
[58] Chen H, Lin H, Huang Q, Huang F, Xu J, Wang B, et al. A novel double-perovskite Gd_2ZnTiO_6: Mn^{4+} red phosphor for UV-based w-LEDs: structure and luminescence properties. J Mater Chem C 2016;4(12):2374–81.
[59] Wang B, Lin H, Xu J, Chen H, Wang Y. $CaMg_2Al_{16}O_{27}$:Mn^{4+}-based red phosphor: a potential color converter for high-powered warm W-LED. ACS Appl Mater interfaces 2014;6(24):22905–13.
[60] Li W, Zhang H, Chen S, Liu YL, Zhuang JL, Lei BF. Preparation and properties of carbon dot-grafted $CaAl_{12}O_{19}$:Mn^{4+} color-tunable hybrid phosphor. Adv Opt Mater 2016;4(3):427–34.
[61] Chen YH, Lei BF, Zheng MT, Zhang HR, Zhuanga JL, Liu YL. A dual-emitting core–shell carbon dot–silica–phosphor composite for white light emission. Nanoscale 2015;7:20142–8.